Review on Gaseous Detectors and Feasibility study of straw tube detector for CBM - Muon Chamber

Project report submitted for the degree of
Master of Science
By
Shubham Jaiswal
Roll No. BICU/PSc/2017-19/02

Supervisor
Dr. Saikat Biswas

DEPARTMENT OF PHYSICS
BOSE INSTITUTE
2019

Acknowledgement

I would like to thank my project supervisor, Dr. Saikat Biswas, for his mentorship and encouragement throughout the process. I am sincerely grateful for his guidance and support during the period of this work and most of all, his patience and understanding.

I would like to thank Prof. Rajarshi Ray for his help, engaging discussions and patience during the entire M.Sc. course. I am equally obliged to Dr. Supriya Das and Dr. Sidharth K. Prasad for their valuable suggestions and lectures that helped me a lot to complete my report. I duly acknowledge the significant role played by Prof. Sanjay K. Ghosh and Prof. Sibaji Raha, in the form of their guidance and discussions during the course.

I would also render sincere gratitude to my seniors including Ms. Shreya Roy, Mr. Sayak Chatterjee, and Mr. Arindam Sen for helping me in all possible ways to analyze the results of my experiments and to understand the basic physics of the detectors.

I am grateful towards my classmates, Mr. Raja Khatri, and Mr. Alex Antony, for their valuable comments, criticisms, and suggestions during the entire duration of the project. For their focused discussions and constructive criticisms, I would also extend gratitude towards Ms. Debonita Saha, Ms. Aayushi Paul, Ms. Krishna Nivedita G, Mr. Abhishek Roy, and Ms. Rituparna Banerjee.

I genuinely thank the staff of Bose Institute in helping to furnish the requisites in my experimental setup.

Last, but not least I would like to thank my parents for their patience and constant support and unhindered belief.

Abstract

The project involves a detailed study to know about the past, present and the future aspects of gaseous detectors used in High energy physics experiments whereas the main focus is on Straw tube detectors. Review of different kind of gaseous detectors are given in the first two chapters. The third chapter contains description of different electronic modules. Details of straw tube is described in Chapter 4. The summary and discussion are presented in the last chapter. Straw tube detectors have widely been used as tracking devices in particle and heavy-ion physics experiments for low material budget. The straw tube is a strong candidate for tracking purpose in the Muon Chamber (MUCH) at Compressed Baryonic Matter (CBM) experiment at the Facility of Antiproton and Ion Research (FAIR). This brings the strict necessity to know the detail characteristics of this type of detectors. The systematic study has been carried out in terms of its variation in gain, energy resolution and other parameters with voltage, using a straw tube detector prototype with 6 straws of diameter 6 mm and length 20 cm. Long-term stability of this detector has been carried out with Argon, CO_2 gas mixture using a Fe^{55} X-ray source. Detailed of the test setup and results are presented in this report.

Contents

List of Figures

1 Introduction to Particle Detectors

In experimental and applied particle physics, nuclear physics, and nuclear engineering, a particle detector, also known as a radiation detector, is a device used to detect, track, and identify ionizing particles, which are produced by nuclear decay, cosmic radiation, or by the experiments with a particle accelerator. Detectors can measure the particle energy and other properties such as momentum, spin, charge, particle type, in addition to merely registering the presence of the particle.

1.1 Introduction

The need of particle detectors practically felt with the discovery of radioactivity by Henri Becquerel in the year 1896. He noticed that the radiation emanating from uranium salts could blacken photosensitive paper. Almost at the same time X rays, which originated from materials after the bombardment by energetic electrons, were discovered by Wilhelm Conrad Röntgen. Thus, the history of particle detectors started more than 100 years ago. The first nuclear particle detectors (X-ray films) were thus extremely simple. Also the zinc-sulfide (ZnS) scintillators in use at the beginning of the last century were very primitive. In 1903, Sir William Crookes experimenting in total darkness with a very expensive radioactive material, radium bromide, first saw flashes of light emitted from the radium salt. He had accidentally spilled a small quantity of this expensive material on a thin layer of activated (ZnS). To make sure he recovered every single dot of it, using a magnifying glass he noticed emissions of light occurring around each tiny grain of the radioactive material. This phenomenon was caused by individual α particles emitted from the radium compound, striking the activated (ZnS). The flashes of light were due to individual photons caused by the interaction of α particles in the zinc-sulfide screen. A particle detector based on this effect, the spinthariscope, is still in use today for demonstration experiments [10].

Photographic films and scintillation screens using the bare human eyes as light detection system helped in the early days of nuclear physics to uncover the mysteries of radioactivity. Photographic emulsions, cloud chambers and later bubble chambers made particle tracks directly visible and let to the discoveries of the positron in 1932 and the pion in 1947 and many new hadronic particles in the following decades. Development of the first electronic detectors started with the invention of the Geiger-Müller tube based on gas amplification principles to measure charged particles by their ionization. Later, scintillation counters were equipped with photo-multiplier tubes (PMTs) to gain much higher sensitivity. Electronic detectors were equipped

with more and more channels, finer granularity and fast data read-out which eventually marked the end of the big bubble chamber era. At the same time, first idea on the use of semi-conductor devices as high precision tracking detectors emerged which formed a third major detector line beside the well established gaseous detectors and photo detectors. Today, these basic detector technologies are even combined into hybrid detector systems such as Silicon PMTs, Micro-pattern Gas Detectors (MWGD) with Pixel readout or Silicon Tungsten calorimeters [9].

1.2 Classification of Detectors

Detection of radiation is entirely possible due to the interaction of radiation with the matter. As a result of interaction, photons, electron-ion or electron-hole pairs are produced in the detector medium. Depending on the active medium and detection techniques, detectors are broadly classified into three groups:
1) Gaseous detectors
2) Scintillation detectors
3) Semiconductor detectors

1.2.1 Gaseous Ionization Detectors:

Gaseous Ionization Detectors worked on the basis of the ionising effect of radiation in the gaseous medium. If a particle has enough energy to ionize a gas atom or molecule, the resulting electrons and ions cause a current flow which can be measured. Gaseous ionisation detectors form an important group of instruments used for radiation detection and measurement. Since my project is mainly based to this type of detectors, it has been explained in detail in section 2.

1.2.2 Scintillation Detectors

A charged particle passing through matter will create electron-ion pairs in a gas and electron-hole pairs in a semiconductor. In some substances it may result in excitation of the atoms of molecules. Those substances in which the molecules de-excite by emitting a photon are known as scintillators. If a photon excites the molecules of a substance, which then de-excite by emitting a lower energy photon, the substance is said to fluoresce. Absorption and emission occur over a wide range of photon energies, which can overlap, leading to unwanted self-absorption. The greater the difference between the main absorption and main emission energies, the less the amount of self-absorption.

The scintillation detectors are further classified on the basis or scintillating material used [2].

Table 1: Organic versus inorganic scintillators

Scintillator	Composition	Density (gcm^{-3})	Examples	Notes
Organic	Carbon based (often with benzene)	1.03-1.20	Polystyrene polyvinyl-toluene	Nearly all organic scintillators are plastic since it is cheap and easily moulded.
Inorganic	Non-carbon based crystals	4–8	Sodium iodide Barium fluoride	Higher density makes these useful for total absorption

1.2.3 Semiconductor Detectors:

The high energy physics experiments these days uses silicon detectors as their central tracking detector. The position resolution of this detectors is far more than that which is possible in gaseous ionisation chambers. In semiconductor detectors individual module comprises silicon that has been doped to form a diode. When the module is reverse-biased, a depletion region is set up with an electric-field that sweeps charge-carriers to the electrodes. When a charged particle passes across the silicon strip it will liberate electrons from their atoms creating electron-hole pairs. The electric-field in the depletion region sweeps the new electron-hole pairs to the electrodes where they are collected and that particular module records a 'hit'. In contrast to gaseous detectors, silicon detectors do not track the charged particle through the entire body of silicon - instead individual, isolated mm sized strips or μm sized pixels record hits. Those modules that record hits trace out the path followed by the charged particle. The smaller the modules, the better the spatial resolution and it is around 5 μm for a 300 μm thick module.

The time taken for collection decreases as the bias voltage is increased. Increasing the voltage beyond that value is necessary for complete collection. Over-biasing reduces the collection time further. In a 300 μm thick silicon detector, electrons are

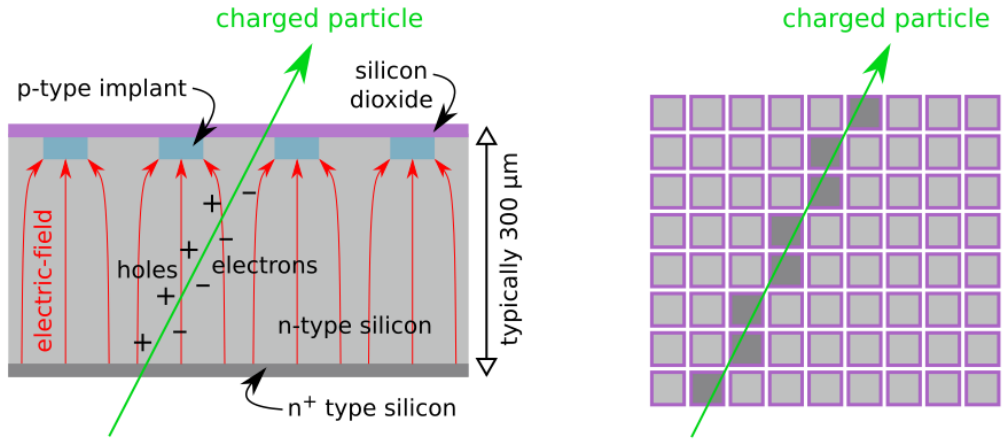

Figure 11: Left: schematic diagram of a silicon detector; Right: an array of silicon detector pixels - those which detected hits are shown highlighted and trace out the particle's trajectory [2].

collected in about 10 ns and holes in about 25 ns.
In contrast to gaseous ionisation detectors, the active material in solid-state detectors is much denser, therefore every effort is made to make the silicon as thin as possible - otherwise any improvement in resolution gained by using silicon, is negated by the effects of increased multiple scattering. Hence the increased spatial resolution possible with silicon detectors (compared to gaseous ionisation detectors) comes at an increased cost. Schematic diagram of a silicon detector in figure 1.1 (left) and an array of silicon detector is shown in figure 1.1 (right) [2].

1.3 Project Objective/Aim

The main objective of this project is to get a thorough understanding of Gaseous particle detectors, i.e., the various aspects of physics involved in its operation. And then to perform the study, experiment and the experimental data analysis for the straw tube Detector to study the feasibility if it for the third and fourth stages of CBM Muon Chamber (MUCH) Experiment. Triple GEM detectors will be used in the first two stations of CBM-MuCh. MuCh is one of the largest components of the CBM experimental setup. It is designed to identify muon pairs which are produced in high-energy heavy-ion collisions in the beam energy range from 4 to 40 AGeV (GeV per nucleon) [11].
In the CBM experiment at FAIR, Germany, we will explore the QCD phase diagram at moderate baryonic density. Muon chamber will use several hadron absorbers made of graphite and iron and sophisticated gaseous detectors [7].

2 Gaseous Detectors

2.1 Principle

A gaseous detector is a sealed chamber with two electrodes filled by suitable gas. We considered a cylindrical chamber with a central anode wire. The wall of the cylinder acts as cathode. The schematic of a cylindrical gaseous detector is shown in Figure 2.1.

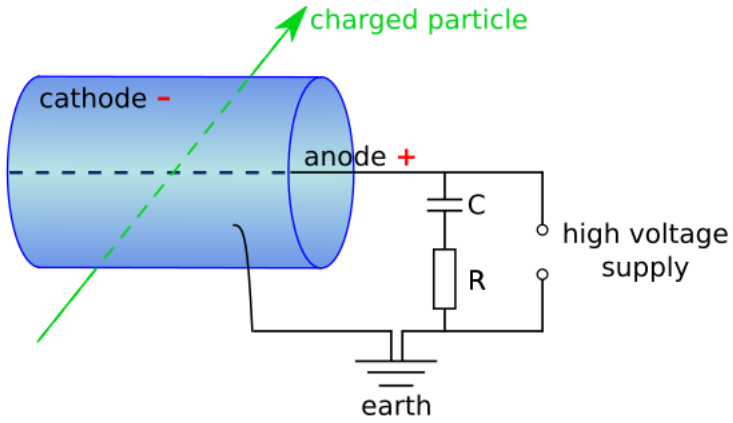

Figure 21: Circuit diagram for a gaseous ionisation chamber.

A positive voltage is applied to the central wire (anode) and the chamber walls (cathode) to create an electric field between them. When a charged particle passes through the chamber it ionises the gas molecules creating negative electrons (anions) and positive ions (cations) along its path. The collection of these charged particles reduces the voltage across the capacitor - this in turn increases the voltage across the resistor. This time varying voltage also called a 'pulse' across the resistor is recorded electronically, registering a hit.
The height of the pulse can be calculated as follows:

- The charge, Q on a capacitor of capacitance C under voltage V is given by:

$$Q = CV$$

- A change in the charge causes a change in the voltage:

$$\Delta V = \frac{\Delta Q}{C}$$

- The change in charge is equal to the number of electrons collected by the anode. This is related to the number of ionising events that occur (let it be 'n') as the charged particle being detected after passing through the gas. If the ionisation products have sufficient energy to cause secondary ionisations, then the charge due to the primary ionisation events ($n \times e$) must be multiplied by the gas amplification factor A:

$$Pulse\ height = \Delta V = \frac{Ane}{C}$$

- The gas amplification factor, A, is dependent on the voltage applied.

As shown in above equation, the pulse height depends on the number of ion pairs collected by the anode. However, the number of ion pairs collected depends on the applied voltage [2]. According to the applied voltage the operation of gas detector is divided into several regions as described in the following section.

2.2 Regions of Operation

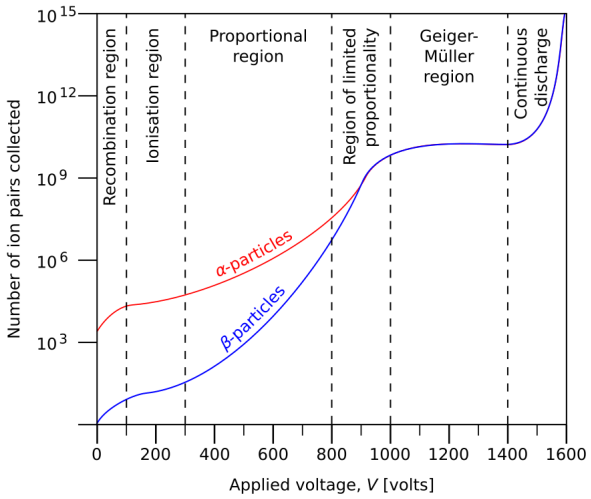

Figure 22: Number of ion pairs collected versus applied voltage in a gaseous ionisation chamber.

The number of ion pairs collected at the respective electrodes varies as the voltage applied to the detector is increased. In Figure 2.2, two curves are shown for the curve

for α and β particles. From the curves it is clear that the number of electron ion pairs collected for α particle is higher than that of β particle since the primary number of electron ion pairs for α-particles is more because of its larger mass [2].

Recombination region

In this region, the voltage is insufficient to create an electric field strong enough for collection of all the ions produced. Instead they drift very slowly towards the electrodes and recombine back to neutral molecules before they can be collected. And as the voltage is increased - more ions are collected, but until the saturation value is reached, not all ions will be prevented from recombining. For this reason gaseous ionisation chambers are not operated at these voltages.

Ionisation region

When Voltage is increased further, around 100 V a saturation value is reached i.e., the voltage is now sufficient to ensure collection of all the ion pairs that the charged particle creates. However, the voltage is not yet strong enough to cause secondary ionisation there is no gas amplification here, hence there is no rise in the number of ions collected.

Proportional region

In this region, current increases again with the voltage but now the electric field is strong enough to accelerate free electrons to the energy where they are also capable of ionizing gas molecules in the cylinder. The electrons liberated in these secondary ionizations then accelerate to produce still more ionization and so on. This results in an ionization avalanche. This avalanche occurs very quickly and almost entirely within a few radii of this wire since the electric field is strongest near the anode. The number of electron-ion pairs in the avalanche is directly proportional to the number of primary electrons, that results then is a proportional amplification of the current, with a multiplication factor depending on the working voltage V. This factor can be as high as 10^6 so that the output signal is much larger than that from an ionization chamber, but still in proportion to the original ionization produced in the detector. This region of proportional multiplication extends up to some point and a detector operating in this domain is known as a proportional chamber [1][9]. Since the straw tube operates in this region, further discussion is done in section 2.4 .

Region of limited proportionality

If the voltage is now increased further, the total amount of ionization created through multiplication becomes sufficiently large that the space charge created distorts the electric field about the anode. Proportionality thus begins to be lost. This is known as the region of limited proportionality [1].

Geiger-Muller region

Increasing V still higher, the energy becomes so large that a discharge occurs in the gas. Because instead of a single, localized avalanche at some point along the anode wire (as in a proportional counter), a chain reaction of many avalanches spread out along the entire length of the anode is triggered. These secondary avalanches are caused by photons emitted by deexciting molecules which travel to other parts of the counter to cause further ionizing events. The output current thus becomes completely saturated, always giving the same amplitude regardless of the energy of the initial event. In order to stop the discharge, a quenching gas must be present in the medium to absorb the photons. Detectors working in this voltage region are called Geiger-Muller or breakdown counters. The Geiger voltage region is characterized by a plateau over which the count rate varies little. The width of the plateau depends on the effectiveness of the quencher in the gas [1].

Region of continuous discharge

If the voltage is increased further above that of Geiger-Muller region, the voltage is so high that once ionisation occurs there is a continuous discharge of electricity. The Geiger plateau is the last useful range for continuously applied voltages, anything above this cannot be used for particle detection [2].

2.3 Passage of radiation through Detector

The basic interactions of radiation with the matter is discussed in the following section. The understanding of these interactions is essential for building any detector. For charged particles and photons, the most common processes by which they lose energy are by the electromagnetic interactions. For the neutron, however, processes involving the strong interaction will preferentially occur, although it is also subject to electromagnetic (through its magnetic moment) and weak interactions as well.

2.3.1 Energy Loss of Heavy Charged Particles by Atomic Collisions

when charged particles pass through the matter they loss energy and deflect from its incident direction. The main processes involved are:

1. Inelastic collisions with the atomic electrons of the material
2. Elastic scattering from nuclei.
3. Emission of Cherenkov radiation
4. Nuclear reactions
5. Bremsstrahlung.

The cross section for the last three processes are small compared to the first two mentioned precesses. Let us consider two classes of particles based on their masses: (1) Light particles i.e., electron and positron (2) Heavy particles. Inelastic collision is mainly responsible for the loss of energy of heavy particles. Transfer of energy from the particle to the atom causes ionization or excitation of the latter. The amount transferred in each collision is generally a very small fraction of the particle's total kinetic energy. These atomic collisions are divided into two groups:
(1) Soft collisions, in which only an excitation occurs, and
(2) Hard collisions in which the energy transferred is sufficient for ionization. In some of the hard reactions, enough energy is transferred such that the electron itself causes substantial secondary ionization. These high-energy recoil electrons are sometimes referred to as δ-rays or knock-on electron. Elastic scattering from nuclei also occurs frequently although not as often as the collision with atomic electrons. The inelastic collisions are statistical in nature, occurring with a certain probability. However, because their number per macroscopic path length is generally large, the fluctuations in the total energy loss are small and one can meaningfully work with the average energy loss per unit path length. This quantity, often called the stopping power or simply dE/dx. It was first calculated by Bohr using classical arguments and later by Bethe, Bloch and others using quantum mechanics [1].

2.3.2 Quantum mechanical result of Energy loss: The Bethe- Bloch formula

In the classical approach by Bohr, electron is assumed free and initially at rest and it moves very slightly during the interaction with the heavy particle so that the electric field acting on the electron may be taken at its initial position. Moreover,

after the collision, we assume the incident particle to be essentially undeviated from its original path because of its much larger mass ($M \gg m_e$). This is one reason for separating the electrons from heavy particles. Then the Gauss' Law and impact parameter concepts were used to calculate the value of stoping power.

But in the quantum mechanical calculations energy transfer is parametrized in terms of momentum transfer rather than the impact parameter. This, of course, is more realistic since the momentum transfer is a measurable quantity whereas the impact parameter is not.
The energy loss per unit length of a relativistic charged particle is given by:

$$-\frac{dE}{dx} = 2\pi N_a r_e^2 m_e c^2 \frac{Z}{A}\frac{z^2}{\beta^2}\left[\ln\left(\frac{2m_e\gamma^2\mu^2 W_{max}}{I^2}\right) - 2\beta^2\right]$$

with
$2\pi N_a r_e^2 m_e c^2 = 0.1535\ MeVcm^2/g$
r_e : classical electron radius = 2.817 x 10$^-$13 cm
m_e : electron mass; N_a : Avogadro's number; I : mean excitation potential; Z : atomic number of absorbing material; A : atomic weight of absorbing material; ρ : density of absorbing material; z : charge of incident particle in units of e; $\beta = c/v$ of incident particle; $\gamma = 1/\sqrt{1-\beta^2}$; W_{max} : maximum energy transfer in a single collision.

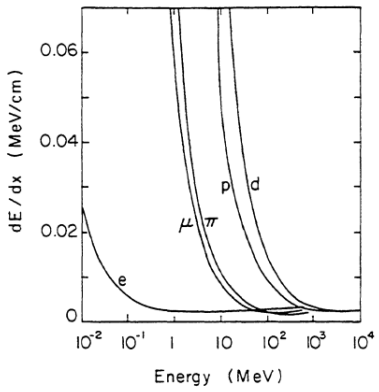

Figure 23: Energy loss per unit length in air, computed from Bethe-Bloch formula, for different particles as a function of their energy [3].

The differential energy loss depends only on the projectile velocity β and charge of the particle but not on its mass. The Energy loss per unit length in air, computed

from Bethe-Bloch formula, for different particles as a function of their energy is presented in the Figure 2.3.

2.3.3 The Energy Loss Distribution

We have discussed energy loss in terms of the mean energy loss suffered by charged particles when passing through a matter. For any given particle, however, the amount of energy lost will not, in general, be equal to this mean value because of the statistical fluctuations which occur in the number of collisions suffered and in the energy transferred in each collision. An initially mono-energetic beam, after passing through a fixed thickness of material, will therefore show a distribution in energy loss .

Calculation of the distribution of energy losses for a given thickness of absorber is a difficult mathematical problem and is generally divided into two cases: thick absorbers and thin absorbers. For **thick absorbers** the number of collisions is large, the energy loss distribution will be Gaussian in form.This follows directly from the Central Limit Theorem in statistics which states that the sum of N random variables, all following the same statistical distribution, approaches that of a Gaussian distributed variable in the limit of $N \to \infty$. If we take our random variable to be δE, the energy lost in a single atomic collision, and assume that the energy lost in each collision is such that the velocity of the particle is negligibly altered (so that the velocity-dependent collision cross-section stays constant), then the total energy lost is the sum of many independent δE, all randomly distributed. Assuming there are a sufficient number of collisions N, then the total will approach the **Gaussian** form,

$$f(x, \Delta) \propto exp\left(-\frac{(\Delta - \bar{\Delta})^2}{2\sigma^2}\right)$$

where, x is thickness of absorber; Δ is energy loss in absorber; $\bar{\Delta}$ is mean energy loss; σ is standard deviation.

On the other hand for the **Thin absorber** the number of collisions N is too small that the the Central Limit Theorem is not applicable. This is because of the possibility of large energy transfers in a single collision. For heavy particles, the maximum energy transfer in a single collision is kinematically limited, while for electrons, as much as one-half the initial energy can be transferred. In this latter case, there is also the additional possibility of a large "one-shot" energy loss from bremsstrahlung as well. While these events are rare, their possibility adds a long tail to the high energy side of the energy-loss probability distribution thus giving it a skewed, asymmetric form. Note that in the Figure 2.4, the mean energy loss no longer corresponds to the peak but is displaced because of the high energy tail.

In contrast, the position of the peak now defines the most probable energy loss. These two quantities may be used to parametrize the distribution. In this type of

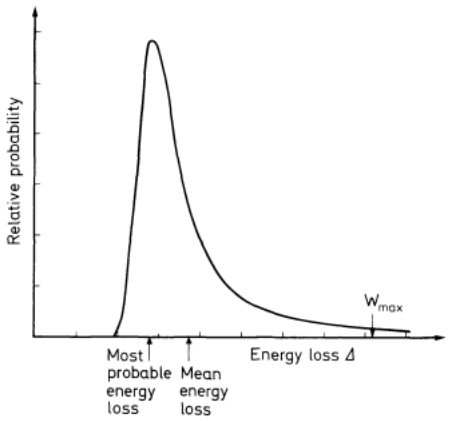

Figure 24: Typical asymmetric distribution of energy loss in a thin absorber with a long high energy tail.

distributions the distinguishing parameter is the ratio between the mean energy loss and the maximum energy transfer allowable in a single collision.i.e.,

$$\kappa = \frac{\bar{\Delta}}{W_{max}}$$

The peculiar shape of the energy loss distribution can be written as:

$$f(\lambda) = \frac{1}{\sqrt{2\pi}} e^{-\frac{1}{2}(\lambda + e^{-\lambda})}$$

where the energy variable λ represents the normalized deviation from the most probable energy loss $(\Delta E)_{MP}$:

$$\lambda = \frac{\Delta E - \Delta E_{MP}}{\xi}, \quad \xi = K \frac{Z}{A} \frac{\rho}{\beta^2}$$

Where, Z, A and ρ the medium's atomic number, mass and density, in the CGS system of units $K = 0.308 MeV g^{-1} cm^2$ [1][3].

2.3.4 Drift and Diffusion of charges in gases

Ions and electrons forms in a gas when radiation passes through it, lose their energy in multiple collisions with surrounding molecules and acquire the thermal energy distribution of the medium. Under the action of moderate external electric fields, charges move through the medium while diffusing, until neutralized either by recombination in the gas or at the walls. For ions, a process of charge transfer is possible with a molecule of its own gas or of another elements having lower ionization potential. Electrons, wandering in the gas and colliding with the molecules, can be neutralized by a positive ion, attach to a molecule having electron affinity, or get absorbed at the walls of the containment vessel. The physical quantities like mobility, drift velocity, diffusion etc., depends on the gas density, temperature, pressure etc. The dependancy of the quantities mentioned above is discussed in the following sections.

Thermal diffusion of ions

In the absence of external electric field and magnetic field and inelastic collision processes, ions and electrons can be treated using classical kinetic theory of gases. Probability of an atom or molecule having an energy ϵ at temperature T is given by Maxwell-Boltzmann law:

$$F(\epsilon) = 2\sqrt{\frac{\epsilon}{\pi(kT)^3}}e^{-\frac{\epsilon}{kT}}$$

where, k is Boltzmann's constant, equals $1.38 \times 10^{16} erg/^oK$ or $8.617 \times 10^{-5} eV/^oK$; By interaction of above function we get the average thermal energy

$$\bar{\epsilon_T} = kT$$

at normal conditions, $\epsilon_T = 0.025$ eV

The corresponding distribution of velocity v for a particle of mass m is:

$$f(v) = 4\pi \left(\frac{m}{2\pi kT}\right)^{\frac{3}{2}} v^2 e^{-\frac{mv^2}{2kT}}$$

Thus, for the average velocity,

$$\bar{v} = \int_0^\infty v f(v) dv = \sqrt{\frac{8kT}{\pi m}}$$

and the most probable value of velocity will be,

$$v_{MP} = \sqrt{\frac{2kT}{m}}$$

A localized distribution of molecules or ions diffuses symmetrically by multiple collisions following a Gaussian law:

$$\frac{dN}{N} = \frac{1}{\sqrt{4\pi Dt}} e^{-\frac{x^2}{4Dt}} dx$$

where, dN/N is the fraction of particles found in the element dx at a distance x from the origin and after a time t; D denotes a diffusion coefficient [12].
This expression can be used to estimate the time-dependent dilution in a gas volume of a given species. The root mean square of the distribution, or standard deviation, is given for linear and volume diffusion, respectively, by:

$$\sigma_x = \sqrt{2Dt} \text{ and } \sigma_v = \sqrt{6Dt}$$

Thus, we can say that gases with lower mass are faster as compared to the heavy gases. This, will give us some idea about which ion will diffuse by what rate in a medium of particular gas. There is two thing velocity distribution and space distribution, for lighter gases velocity distribution will be broader i.e., the most probable velocity will be of higher value so diffusion will be faster. This suggests that the space distribution will become flat in lesser time for lighter gases as compared to heavier gases [12].

Ion mobility and diffusion in an electric field

On application of electric field, there will be a net movement of ions in the field direction (it is different from motion due to thermal energy). The drift velocity(w^+) is proportional to the electric field applied. So, defining mobility as,

$$\mu = \frac{w^+}{E}$$

In terms of pressure and temperature,

$$\mu(P,T) = \frac{T}{T_0}\frac{P_0}{P}\mu(P_0,T_0)$$

For ions mobility becomes constant for higher electric fields, but not for electron.

By classical Nernst-Townsend formula for ideal gas, in which moving charges remain in thermal equilibrium, we have

$$\frac{D}{\mu} = \frac{kT}{e}$$

where, D is the diffusion coefficient, and e the electron charge. Now, Replacing 'D'in expression of standard deviation we get,

$$\sigma_x = \sqrt{\frac{2\mu kTt}{e}} = \sqrt{\frac{2w^{+}kTt}{Ee}}$$

or,

$$\sigma_x = \sqrt{\frac{2kTx}{eE}}$$

Thus, the space diffusion does not depend on the type of ion and pressure, but only on the field. Mobility of a migrating gas of molecular weight M_I in a gas of molecular weight M_M is given by **Langevin's law**,

$$\mu_I = \sqrt{\left(1 + \frac{M_M}{M_I}\right)}$$

In a mixture of gases $G_1, G_2, ..., G_N$ the mobility μ_i of the ion G_i is given by the relation (Blanc's law):

$$\frac{1}{\mu_i} = \sum_{j=1}^{n} \frac{p_j}{\mu_{ij}}$$

where, p_j is the volume concentration of gas j in the mixture, and $\mu_i j$ the mobility of ion G_i in the gas G_j [12].

Some points should be noted :

- Compared to their thermal velocities, the drift speed of the ions is slow, however, for electrons this can be much higher since they are much lighter.
- For positive ions, the drift velocity is found to depend linearly on the ratio E/P, (also known as the **Reduced Electric Field**), up to relatively high electric fields.
- Unlike positive ions, the mobility for electrons is much greater and is found to be a function of E. Velocities as high as a few times 10^6 cm/s can generally be attained before saturation sets in. The electric fields at this point are generally on the order of 1 kV/cm-atm.
- If the mean energy of the electrons exceeds thermal energies, the diffusion constant D then increases accordingly causing a greater spread of the electron cloud. This has important consequences for detectors such as the drift chambers which attempt to determine the position of a track by measuring the drift time of the ionization electrons [1].

- The ion's clearing time is almost independent of the gas used because the value of mobility for most of the light ions are similar [12].

2.3.5 Avalanche Multiplication

Multiplication in gas detectors occurs when the primary ionization electrons gain sufficient energy from the accelerating electric field to also ionize gas molecules. The resulting secondary electrons then produce tertiary ionization and so on. This results in the formation of an avalanche. This exponentially increases the number of charges collected and consequently modifying the amplitude and time development of the detected signals. Because of the greater mobility of the electrons, the avalanche has the form of a liquid-drop with the electrons grouped near the head and the slower ions trailing behind as shown in Figure 6.

If λ is the mean free path of the electron for a secondary ionizing collision, then $\alpha = 1/\lambda$ is the probability of an ionization per unit path length. This is better known as the **first Townsend coefficient**. Figure shows the coefficients for different gases. If there are n electrons, then for a path length dx,

$$dn = n\alpha dx$$

where dn is the number of new electrons created. So, for length of path x, we have,

$$n = n_0 exp(\alpha x)$$

where n_0 is the original number of electrons. The multiplication factor is then

$$M = n/n_0 = exp(\alpha x)$$

In the case of nonuniform electric fields, α is a function of x. so,

$$M = exp\left[\int_{r_1}^{r_2} \alpha(x)dx\right]$$

The largest value of M physically possible is 10^8 after which breakdown occurs. This is known as Raether limit. The multiplication factor or gas gain is of fundamental importance for the development of proportional counters [1][12].

2.4 Proportional Counter

In this section, a more sophisticated tracking detector will be discussed. The ionization chamber and Geiger counter are not widely used in current physics experiments

and are generally found as radiation monitoring and survey instruments. The basic feature of the proportional counter is the proportional gas multiplication which occurs in it. Its geometry plays an important role to make it useful. Since geometry is responsible for the electric field distribution.

For a planar detector consisting of a parallel anode and cathode plates with gas filling in between. The electric field is thus uniform and perpendicular to the plates. By the application of high enough voltage, the electrons created in an ionizing event will be accelerated towards the anode plate triggering avalanches along its path. In this case, the total ionization produced will depend on the length of the path and thus on where the ionizing event occurs. For events with the same energy, therefore, the signal amplitude will vary with position and the relation between signal and energy is lost. This problem is solved by using a cylindrical geometry because of 1/r dependence of electric field, the field becomes intense very close to the surface of the anode wire. If the voltage is correctly chosen, ions and electrons will simply drift towards their respective electrodes. Only when the electrons are very close to the anode wire (a few wire diameters) does the electric field become intense enough for multiplication to occur and while approaching the anode the mean free path for multiplication decreases. Thus, the avalanche occurs very quickly and the signal is generated. Now, all multiplications take place in a small region about the anode.

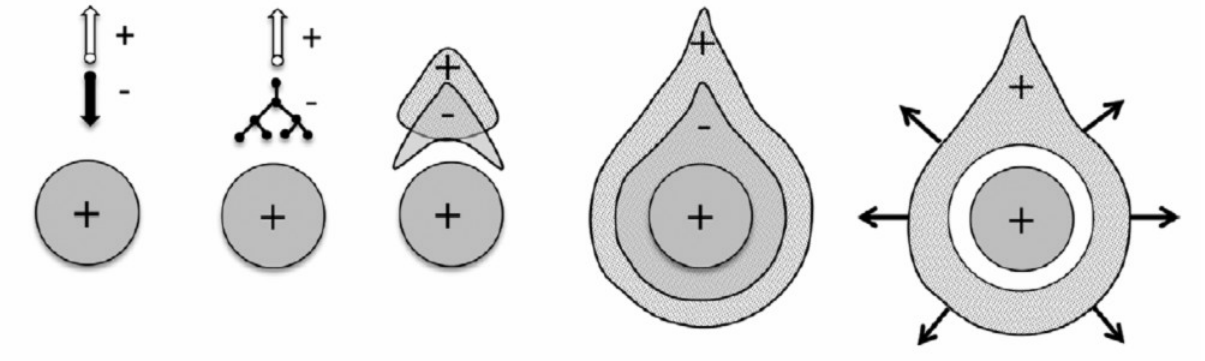

Figure 25: Avalanche growth around a thin wire [12].

The avalanche takes on a drop-like form. As the drop approaches the anode wire, diffusion of the charges causes the drop to surround the wire in the azimuthal direction as shown in the Figure 2.5. The electrons are then collected very quickly ($\approx$1 ns) while the positive ions begin drifting towards the cathode. This ion drift is mainly responsible for the signal seen on the electrodes [1][9].

Gain calculation for cylindrical proportional detector:

General form of mean gas amplification factor M for a cylindrical proportional detector can be written as,

$$M = exp\left[\int_a^{r_c} \alpha(r)dr\right]$$

Where r is the radius from the anode wire and r_c is radius beyond which field is too low to support gas amplification. For the case of nonuniform electric fields, αwill be function of electric field (E), and can be written normally as,

$$\ln M = \int_{E(a)}^{E(r_c)} \alpha(E)\frac{\partial r}{\partial E}dE$$

In a cylindrical proportional tubes, E is given by

$$E(r) = \frac{V}{r\ln(b/a)}$$

Where,
V = voltage applied between anode and cathode,
a = anode wire radius,
b = cathode inner radius.

$$\ln M = \frac{V}{\ln(b/a)}\int_{E(a)}^{E(r_c)} \frac{\alpha(E)}{E}\frac{dE}{E}$$

Assuming linearity between α and E, expression of M will be look like,

$$M = Ae^{BV}$$

Where, A and B are constants.

2.4.1 Time development of Signal

Basic concepts involved are as follows:

- The pulse forms by induction due to the movement of the ions and electrons as they drift towards the cathode and anode, rather than by the actual collection of the charges itself.

- If the movement of the charges is fast relative to the time that an external power supply can react to changes in the energy of the system, we can consider the system as closed. Energy is then conserved. This fact is used to calculate the voltage change induced across the electrode by the displacement of the charge.

- The induced signal is almost entirely due to the motion of the positive charges and one can ignore the motion of the electrons. But the contribution of the electrons can be ignored only if they are all created near the anode. This result can be proved by the mathematical calculation of the induced voltages from electrons and ions separately. It is found that voltage induced by the electrons is less than one percent of voltage induced by ions.

- A typical pulse signal from a cylindrical proportional counter is as shown in the figure. The pulse is usually cut short by an RC differentiating circuit with a time constant τ. The figure shows the effect of two different time constants.

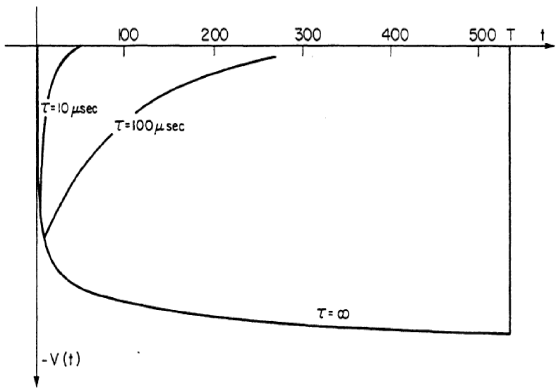

Figure 26: Time development of the voltage pulse in a proportional counter on the anode; T is total drift time of positive ions from anode to cathode. The pulse shape is shown for two differentiation time constants [12].

Due to the high initial velocity of the ions in the field around the anode, the signal growth is very fast at short times, about one half of the signal develops in a fraction of time corresponding to the ratio of the anode wire to cathode radius. With the aim of increasing the rate capability of the counter, pulse is differentiated to shorted duration. Depending on the time constant of the differentiator, the fall time of the resulting pulse will vary [1][12].

.

2.4.2 Proper filling gas

Selection of proper filling gas for the best possible operation of proportional counters is based on following three major aspects:

- **Ionization and drift:** The drifting electrons should not be trapped by the molecules of the gas used so noble gases are usually chosen since they require high excitation energy (11.6 eV for Argon) and require the lowest electric field intensities for avalanche formation. Monoatomic gases are used since they do not have vibrational and rotational modes, only excitation and ionization is possible [1].

- **High gain, stable operation:** Another objective is to get high gain at low voltage, excited atoms formed in the avalanche deexcite giving rise to high energy UV photons (11.6 eV) capable of ionizing the cathode and causing further avalanches. This problem can be remedied by the addition of a polyatomic gases, such as methane or alcohol. A few inorganic gases, such as CO_2 , BF_3 can also be used. These molecules act as quenchers by absorbing the radiated photons and then dissipating this energy through dissociation or elastic collisions, giving gains of the order of 10^6. Often used quencher are isobutane and methane. The gain can still be further increased by adding a judicious amount of electronegative gas such as freon (CF_3Br) or ethyl bromide. Apart from absorbing photons, these gases can also trap electrons extracted from the cathode before they can reach the anode to cause an avalanche. A gain of 10^7 can then be attained. But the recombination of dissociated organic molecules results in the formation of solid or liquid polymers which accumulate on the anode and cathode of the detector. Positive ions reaching the cathode must then slowly diffuse through this layer to be neutralized. Thus inorganic quenchers are better option; however they are much less efficient [1][12].

- **Prevent ageing:** Impurities in the gas (or in the chamber) may form deposits on the wire and reduce the gain. This can be prevented by using clean gas and adding 1% alcohol, water or oxygen.

- **Benefits of flowing gas:** In a sealed gas counters large amount of quencher consumes in each detected event. Thus, changes in the operational characteristics will be observed after certain number events. So for a continuous gas flow this problem can be solved [1].

2.5 Different kinds of Gaseous detectors

The field of the particle gaseous detector is vast. Depending on the need of the particle physics experiments different types of Gaseous detectors have been developed so far, some of them are discussed in this section.

2.5.1 MWPC

A multi-wire proportional chamber (MWPC) is simple and robust detector. It is most useful in a situation in which charged particle tracks have to be detected and localised over a large area. It has time resolution of the order of 25-30 ns for a two mm wire spacing. The basic MWPC consists of a plane of equally spaced anode wires centered between two cathode planes. Typical wire spacings are 2 mm with an anode-cathode gap width of 7 or 8 mm as shown in the Figure 2.7(a).

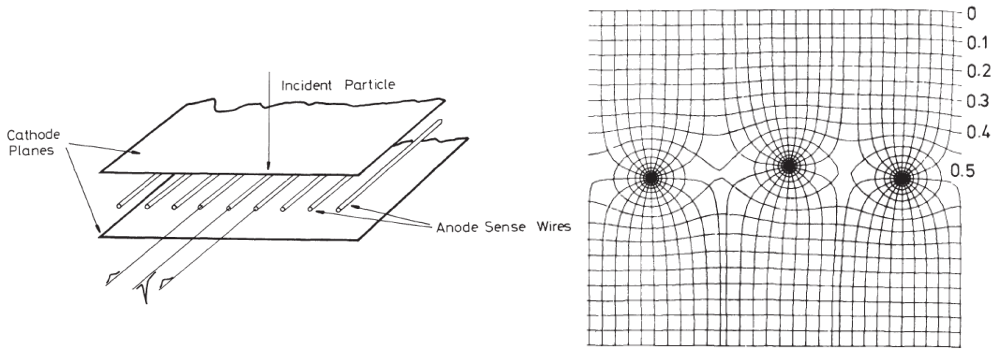

(a) (b)

Figure 27: (a) Basic configuration of a multi-wire proportional chamber; (b) Electric field lines and potentials in a multi-wire proportional chamber. The effect of a slight wire displacement on the field lines is also shown [1]

If a negative voltage is applied to the cathode planes, an electric field configuration as shown in Figure 2.7(b) arises. Except for the region very close to the anode wires, the field lines are parallel and almost constant. Its limitations are due to the wire spacing and the ion mobility. It is difficult to build wire planes with a wire spacing of less than 1 mm due to the electrostatic repulsive forces between the wires. These forces push the wires above and below the plane and make the chamber unstable. This problem can only be avoided by using short wires, which removes much of the

advantages of the MWPC. The low mobility of the positive ions results in a long rise-time for the pulses and in the build-up of an ion cloud around the wires. That results in a poor time resolution and limits the maximal count rate to approximately 10^4 $mm^{-1}s^{-1}$. To overcome these limitations, a number of variants of the standard MWPC or drift chamber have been developed. These devices take advantage of techniques to produce micro-patterns that have been developed over the last decades, mainly for the microelectronics industry [3][1].

2.5.2 MSGC

A Micro-Strip Gas Counter (MSGC) is an ionisation chamber, where the anodes and cathodes consist of thin metallic electrodes deposited on an insulating substrate, usually a glass plate. Very narrow (≈7 μm) anode strips alternate with wider cathode strips (≈100 μm), making a periodic structure with a pitch of typically 200 μm. The anodes are at a positive potential relative to the neighbouring cathode strips.

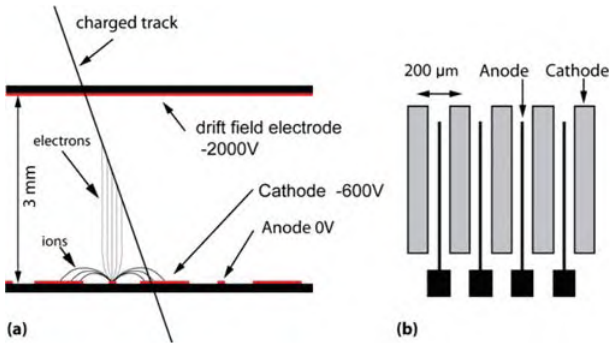

Figure 28: Geometry and typical operating voltages of a MSGC [13].

Photolithography technique is used for the construction of such a fine electrode pattern. Geometry and typical operating voltages of a MSGC is shown is the Figure 2.8. The plane with the anodes and cathodes forms one wall of the gas gap, the other wall is a plane with a fully conductive surface. Both planes together create an electric field that pushes the electrons towards the cathode plane. The gas gap is typically 2 mm wide. Typical trajectories of electrons and positive ions are shown in Figure 2.8(a). Structure of the plane with the anodes and cathodes. The anode strips are about 7 μm wide, the cathode strips 100 μm wide and the periodicity of the structure is 200 μm as shown in Figure 2.8(b) [12]. One of the main limitations of the MSGC, compared to a MWPC, is the small value for maximum gas gain that

can be achieved. This is due to the presence of a strong electric field parallel to the substrate surface. The highest gain that can be achieved is a few 10^3. This is at the limit of what is required to detect the signals from minimum ionising particles. To overcome this limitation, other geometries have been proposed which is discussed in following section.

2.5.3 TPC

The time projection chamber (TPC) is a three-dimensional tracking detector capable of providing information about the points of a particle track along with information on the specific energy loss, dE/dx, of the particle. For this reason, the TPC has been referred to as an electronic bubble chamber. The idea of TPC came from both the MWPC and drift chamber. Its basic structure is shown in the Figure 2.9. It is a large gas-filled cylinder with a thin high voltage electrode at the center. The diameter and length of the cylinder can be as large as two meters. When voltage is applied, a uniform electric field directed along the axis is created and a magnetic field is also applied along the axis. The ends of the cylinder are covered by sector arrays of proportional anode wires arranged as shown in figure. Parallel to each wire is a cathode strip cut up into rectangular segments. These segments are also known as cathode pads.

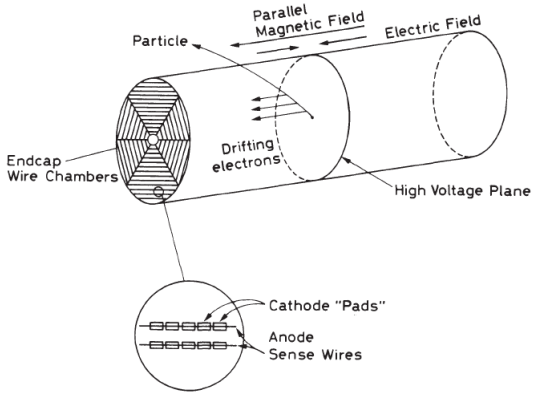

Figure 29: Schematic diagram of a time projection chamber [1].

The detector is positioned so that its center is at the interaction point of the collider. Particles emanating from this point pass through the cylinder volume producing free electrons which drift towards the endcaps where they are detected by the anode wires as in a MWPC. This yields the position of a space point projected

onto the endcap plane. One coordinate is given by the position of the firing anode wire while the second is obtained from the signals induced on the row of cathode pads along the anode wire. The third coordinate, along the cylinder axis, is given by the drift time of the ionization electrons. Since all ionization electrons created in the sensitive volume of the TPC will drift towards the endcap, each anode wire over which the particle trajectory crosses will sample that portion of the track. This yields many space points for each track allowing a full reconstruction of the particle trajectory. Because of the relatively long drift distance, diffusion, particularly in the lateral direction, becomes a problem. This is remedied by the parallel magnetic field which confines the electrons to helical trajectories about the drift direction. Since the charge collected at the endcaps is proportional to the energy loss of the particle, the signal amplitudes from the anode also provide information on the dE/dx of the particle and momentum of the particle is known from the curvature of its trajectory in the magnetic field, then this information can be used to identify the particle [1].

2.5.4 RPC

Resistive plate chambers (RPC) are different type of detector based on the amplification in gases. This detector consists of a gas gap between two planar surfaces and a large voltage of 5–12 kV between the plates. The surfaces are resistive but the back side of the plates is made slightly conductive. If a charged particle passes through the gas gap an avalanche will form. The avalanche will remain localised because the resistivity is very high and the voltage drops immediately to a very low value, preventing further development of the avalanche. The plates of high resis-

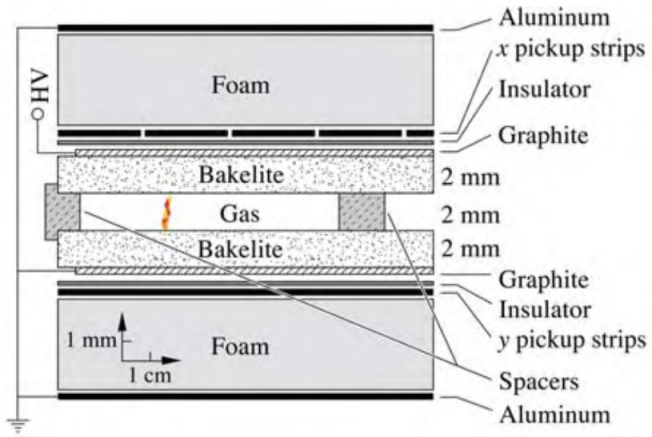

Figure 210: Schematic diagram of a time projection chamber [13].

tivity material of the order of 10^9–10^{13} Ωcm, usually glass or Bakelite plates. The backside of the plates is made slightly conductive with a suitable coating to give it a surface resistivity of the order of 10^5 Ω/square. The unit Ω/square is the usual unit to express surface conductivity. It is the resistivity between two conducting lines on the surface if the distance between the lines is equal to the length of the lines. It is easy to see that this resistivity is independent of the dimension of the square. A typical structure of an RPC is shown in Figure 2.10. To make sure that the gap between the plates remains the same over the whole surface of the detector there are spacers between the plates approximately every 10 cm. Without spacers the electrostatic attraction between the plates would cause the plates to come closer together in the middle. The signal readout is via the metallic pickup strips separated by a thin insulating foil from the slightly conductive coating. The coupling is through the capacitance formed by the pickup strip and the semi-conductive coating. RPC chambers typically have a surface of the order of 1 m^2 and are relatively inexpensive. They produce large signals, up to 300 mV, and allow good timing accuracy (∼1 ns). The rate is limited by the time it takes to recharge the plates at the point where the discharge occurred. This time is quite long, of the order of 1 ms depending on the gain used, but this dead time is limited to the area of less than 1 cm^2 around the discharge point. The rest of the detector remains fully sensitive [13].

2.5.5 MRPC

The Multigap Resistive Plate Chambers (MRPCs) are gas ionization detectors with multiple gas sub–gaps made of highly resistive electrodes having bulk resistivity of 10^{10}– 10^{12} Ωcm, spaced from one another using spacers of equal thickness. These detectors were first developed in 1996. The high voltage (HV) is applied on the outer surfaces of outermost resistive plates to create a uniform and intense electric field across them, while the interior plates are left electrically floating. The external surface of the two outer-most resistive plates are coated with a thin layer of graphite as in RPC. All the electrodes are kept apart by spacers having a bulk resistivity greater than 10^{13} Ωcm. The narrower sub-gaps enhance their time resolution capability. It has been found that a time resolution of less than 100 ps can easily be obtained.

MRPCs is being used by various time of flight (TOF) detector systems (eg. ALICE and STAR) due to their excellent time resolution and higher efficiency for particle detection [18].

The working principle is similar to that of a single gap RPC but in MRPC the additional sub-gaps make the signal collection faster. The internal plates would also allow the detector to withstand a higher operating voltage.

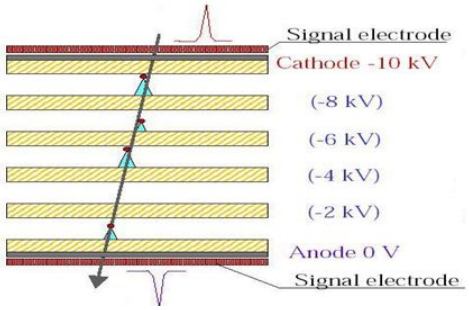

Figure 211: The structure of MRPC.

The structure of a MRPC is shown in Figure 2.11, where all the gas gaps are assumed to be of uniform width. The voltage across each sub-gap is the same. So each sub-gap will produce nearly same number of avalanches when a flux of charged particles passes through it. Avalanche in any of the sub-gaps induce the signals on the electrodes and it will travel very fast to the outer most electrodes, as the inner plates are transparent to the fast signals. The fast signals in case of MRPC are produced by the flow of electrons towards the anode. The resultant signal is the summation from all the gas gaps and it enhances the amplitude of the pulse. The surface resistivity of the conductive graphite coating is high enough so that the electrodes act as dielectrics, i.e., they are transparent to the fast signal generated by the avalanches inside each gas gap. The copper pickup strips placed outside the cathode and anode electrodes collect the signal, through induction. A typical gas mixture, consisting largely of an electronegative gas and small fractions of the quenchers of UV photons and electrons, as used for single gap RPC operation. The intermediate plates also act as the physical barriers for the avalanche growing too big, and hence a higher electric field can be applied to the detector operated in the avalanche mode, making it good in terms of the time resolution and rate capability of the device. The strong uniform electric field stimulates the avalanche process immediately after the primary ionization is created by a charged particle, leading to a very good time resolution. As the number of floating electrodes increases, higher and higher operating voltage is needed to operate it [18].

2.5.6 GEM

The Gas Electron Multiplier detector is a micro pattern gas detector. The main component of this detector is the GEM foil. The GEM foil consists of a kapton foil of 50 μm thick with 5 μm copper cladding surfaces on both sides. Those foils are

pierced with a high density of micro-holes (50 to 100 holes per cm^2) as shown in the Figure 2.12 (left). The most common technique used to produce those holes is the photolithography. Two different techniques of photo-lithography exist to produce GEM foils: Double-Mask and Single-Mask. By applying a potential difference of a few hundred volts between the two planes of copper, produces an electric field of the order of a few tens of kV/cm in the center of the holes as shown in Figure 2.12 (right). In a typical GEM detector the top most electrode is called the drift plane. After that with proper gaps GEM foils are used & the signals are collected from the readout pad. The gap between the drift plane and the top of the 1st GEM foil is called the drift gap. The gap between the bottom of the GEM foil and the readout plane is called the induction gap. When any radiation or charged particle enters into

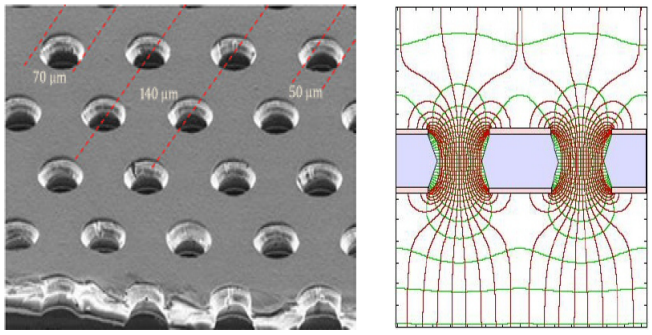

Figure 212: Specification of the GEM foil (Left) &; electric field lines in the GEM holes (right).

the drift region, they first interact with the gas molecules and produce electron-ion pairs. Those electrons are known as primary electrons. Due to the presence of the electric field between the electrode and top of the GEM foil, the primary electrons are accelerated towards the GEM foil. Due to the geometry of the GEM foils, strength of the electric field becomes very high within the holes, and as a result, the primary electrons gain enough kinetic energy to produce there avalanche multiplication by ionizing the gas molecules. Thus after the GEM foil we get large number of electrons. Those electrons are again guided by the field in the other transfer gaps in the case of more then one GEM foil is used, the same multiplication phenomena occurs for other GEM foils and finally the electrons after the last GEM foil is guided to the read out plane by the electric field in the induction gap. Each of the GEM hole works as an individual proportional counter. The ratio between the number of electrons leaving and entering an amplification stage is called the real gain. To increase the gain of the detector without discharge GEM foils can be used in cascaded mode i.e increasing

the number of GEM foils and reducing individual ΔV across a single foil [14].

2.5.7 MicroMegas

MicroMegas are a type of micro-pattern gaseous detector with a spatial resolution below one hundred micrometers. Its basic structure is shown in the Figure 2.13(a). It works on the principle that ionisation electrons created in the conversion gap drift towards the mesh and are transferred through the micromesh to the amplification gap as shown in Figure 2.13(b). In this gap between the mesh and the anode strips,

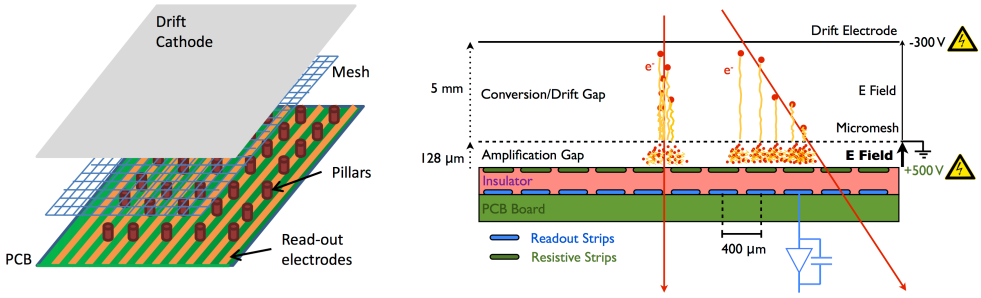

(a) (b)

Figure 213: (a) Structure of the Micromegas. (b) Principle of operation for a MicroMegas [15].

there is a large electric field of the order of 10 kV/cm and this is sufficient to cause electron multiplication and the amplification takes place over the full length of the gap. The anode strips collect the electron cloud, while the positive ions drift in the opposite direction and are collected by the micromesh. Due to the electric field geometry, the average electrons drift over an important fraction of the potential difference, therefore the electron contribution to the signal formation is much larger than with a proportional tube. Because of the much shorter drift time of the positive ions, the signal of the MicroMegas is much faster than the signal of an MWPC.

An important feature of the MicroMegas is the fact that the micromesh is almost transparent to the electrons coming from the conversion gap and stops most of the positive ions coming from the amplification gap. These transparencies depend mainly on the ratio of the field strengths in the amplification and in the conversion gap. Under typical operating conditions, this ratio is large. Hence, almost all electrons are transmitted from the conversion gap to the amplification gap, while only a small fraction of the positive ions is transmitted from the amplification gap to the conversion gap. A gain of 10^5 can be achieved in a MicroMegas chamber [13].

3 Electronic modules

In this we will discuss about the electronics module used to extract information from the radiation detectors. The two most common nuclear instrumentation standard are, Nuclear Instrumentation Module (NIM) and Computed Automated Measurement and Control (CAMAC). The concept of modules in electronic systems offers enormous advantages in flexibility, interchange of instruments, reduced design effort, ease in updating and maintaining the instruments.It provides a common footprint for electronic modules, which plug into a larger NIM bin. The crate must supply 12 and 24 volts DC power to the modules via a back plane, the standard also specifies 6 V DC and 220 V or 110 V AC pins, but not all NIM bins provide them. NIM modules must have a minimum standard width of 1.35 inch (34 mm), a maximum face plate height of 8.7 inch (221 mm) and depth of 9.7 inch (246 mm).
NIM: In this system, the basic electronic apparatus, for example, amplifiers, discriminators, etc., are constructed in the form of modules according to standard mechanical and electrical specifications. These modules, in turn, fit into standardized bins which supply the modules with standard power voltages. Any NIM module will fit into any NIM bin. Pin assignments for NIM standard connector between bin and module is shown in figure 8.

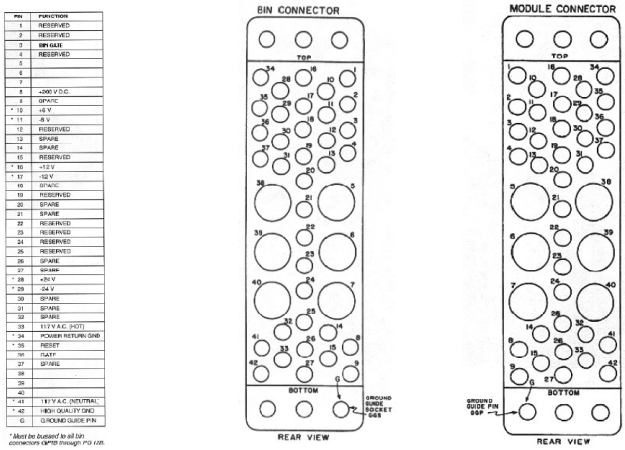

Figure 31: Pin assignments for NIM standard connector between bin and module[12].

3.1 Basic Modules Used

3.1.1 High Voltage Module

High voltage power supply is very important part of any particle detector laboratory. Figure CAEN 4 channel HV programmable power supply module N1470 Regulated high voltage power supply is used to bias any kind of detector. Sometimes multichannel power supply is necessary for a single detector. It basically consists of a step-up transformer that generates the required high voltage. Different detectors require different biasing voltages in the range of a few hundred volts to a few kV. Any desired voltage can be set in the module. The ramp up and ramp down voltages can also be set. For the biasing of anode wire of the straw tube detector CAEN 4 channel HV programmable power supply module N1470 has been used (shown in figure 9). It can supply voltages ranging from 0-8000 Volts.

Figure 32: CAEN 4 channel HV programmable power supply module N1470

3.1.2 Preamplifier

The primary function of a preamplifier is to extract the signal from the detector without significantly degrading the intrinsic signal-to noise ratio, and also to match the impedance between its input and output circuitry. The preamplifier is not designed to give high gain and usually its gain is of the order of 1-10, to amplify weak signals from a detector and to drive it through the cable that connects the preamplifier with the rest of the equipment. Since the input signal at the preamplifier is generally weak, preamplifiers are normally mounted as close as possible to the detector so as to minimize cable length. Three basic types of preamplifier exist,
1) voltage sensitive,
2) current sensitive,
3) charge sensitive,
For Straw tube detector VV50-2 preamplifier is used.

3.1.3 Linear Fan In - Fan Out (FIFO):

Fan-outs are active circuits which allow the distribution of one signal to several parts of an electronics system by dividing the input signal into several identical signals. The fan-in, on the other hand, accepts several input signals and delivers the algebraic sum at the output. These modules may be bipolar, i.e., accepting signals of both polarities, or of single polarity. Both fan-ins and fan-outs come in two varieties: linear and logic. The linear modules accept both analog and logic signals, whereas logic fan-outs and fan-ins are designed for logic signals only. In the case of a logic fan-in, the algebraic sum is replaced by a logical sum (i.e., OR). In our laboratory CAEN Quad linear Fan In - Fan Out module N625 is used (shown in figure 10).

Figure 33: CAEN 4 channel HV programmable power supply module N1470

3.1.4 Discriminator

The discriminator is a device which responds only to input signals with a pulse height greater than a certain threshold value as shown in figure 12. If this criterion is satisfied, the discriminator responds by issuing a standard logic signal; if not, no response is made. The value of the threshold can usually be adjusted manually. The most common use of the discriminator is for blocking out low amplitude noise pulses that has been detected by the detectors. Good pulses, which should in principle be large enough to trigger the discriminator are then transformed into logic pulses for further processing by the following electronics. In this role, the discriminator is

Figure 34: CAEN 8 CH LED module N840

essentially a simple analog-to-digital converter. An important aspect of the discriminator is the method of triggering. Because of its use in timing, it is important that the time relation between the arrival of the input pulse and the issuance of the output pulse be constant. In most discriminators, triggering occurs the moment the pulse crosses the threshold level. This is known as leading edge (LE) triggering. For the study of straw tube detector in this report CAEN 8 CH LED module N840 has been used (shown in figure 11).

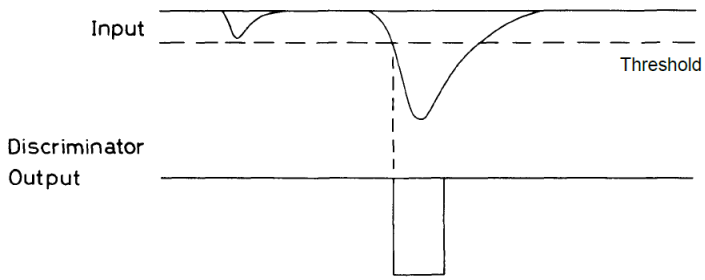

Figure 35: Discriminator operation: only signals whose amplitude is greater than the fixed threshold trigger an output signal.

3.1.5 Single channel Analyzers

The single channel analyzer (SCA) or differential discriminator (DD) is a device which sorts incoming analog signals according to their amplitudes. Like the discriminator, it contains a lower level threshold below which signals are blocked. In addition, however, there is also an upper level threshold above which signals are rejected. Thus only signals which fall between these two levels provoke a response from the SCA, i.e., a standard logic signal. This is illustrated in Figure 13. The opening between the upper and lower level is called the window. With detectors where the output is proportional to energy, the SCA can be used to measure energy spectra by choosing a small, fixed window and systematically sweeping the window across the full pulse height range. The relative number of counts per unit time at each position can then be plotted to give a histogram of the spectrum. The SCA generally has three working modes:
1) Normal Mode or Differential Mode - In this mode, the upper (ULD) and lower (LLD) levels can be adjusted independently of each other, that is the settings of the

LLD has no effect on the setting of the ULD and vice-versa.
2) Window Mode - In this mode one sets the lower level and the window width, that is the distance between lower and upper levels.
3) Integral Mode - Here, the upper level is completely removed from the SCA circuit altogether so that one simply has a discriminator with an adjustable lower level.
In this study Ortec 590A AMP & TSCA module is used.

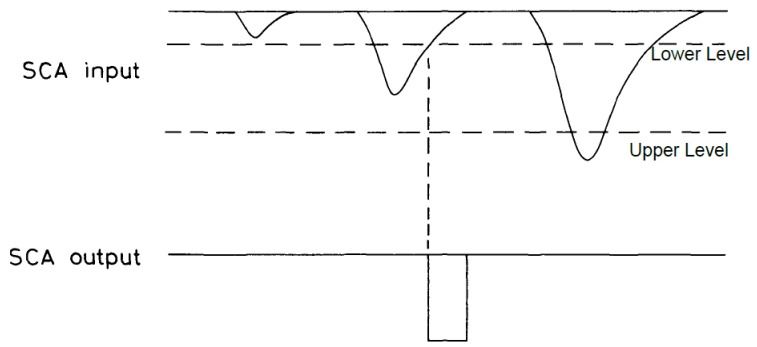

Figure 36: Basic operation of a SCA: only signals whose amplitude fall within the window defined by the upper and lower level threshold trigger an output signal.

3.1.6 Multichannel Analyzers

Multichannel analyzers (MCA) are sophisticated devices which sort out incoming pulses according to pulse height and keep count of the number at each height in a multichannel memory. The contents of each channel can then be displayed on a screen or printed out to give a pulse height spectrum. The MCA works by digitizing the amplitude of the incoming pulse with an analog-to-digital converter (ADC). The MCA then takes this number and increments a memory channel whose address is proportional to the digitized value. In this way incoming pulses are sorted out according to pulse height and the number at each pulse height stored in memory locations corresponding to these amplitudes.

3.1.7 Scalers

The scaler is a unit which counts the number of pulses fed into its input and presents this information on a visual display. So-called blind scalers are those which

do not have their own integrated display. Their contents may be read by a computer or fed into a separate display unit. In general, scalers require a properly shaped signal in order to function correctly; thus it is usually necessary to have a discriminator or a pulse shaper process signals from the detector before they can be counted by the scaler. Scaler can accept NIM or TTL signals as input. In this study CAEN module N1145 Quad scaler and preset counter timer is used.

3.1.8 Digital Storage Oscilloscope

To visualize the signal produced by the detector and study various characteristics of the pulse, such as rise time, fall time, pulse height, pulse shape, etc. Digital Storage oscilloscope (DSO) is used. In the DSO one can set trigger and threshold to encounter only useful events and to cutoff the noise respectively. The DSO used in this project is from Agilent Technologies, model number DSO6054A and can support up to four different input signal ports.

4 Characterization of straw tube detector

4.1 Introduction

Facility for Anti Proton and Ion Research (FAIR) is a upcoming international accelerator facility for the research with antiprotons and ions, under construction at Darmstadt in Hesse, Germany. The Compressed Baryonic Matter (CBM) experiment at FAIR is designed to explore the QCD phase diagram in the region of moderate baryon densities. In CBM experiments there will be different kind of sub-detectors, including highly segmented and fast gaseous detectors. One of the large sub-detectors is the muon-chamber (MUCH) to detect di-muon produced from low mass vector meson. Keeping in mind the high interaction rate at FAIR, the Muon Chamber (MUCH) detector will use Gas Electron Multiplier (GEM) in the first two stations. We are exploring the possibility of straw tubes for the 3^{rd} and 4^{th} stations of CBM-MUCH [5][17][6][7].

A straw tube detector is a single wire gaseous detector operated in proportional mode. It is a tube with diameter 6-8 mm, with a wire stretched along the axis of the tube. The filled gas becomes ionized when a radiation passes through it. A potential difference is maintained between the wire and the walls of the tube, so that when the gas is ionized electrons move in one direction and ions in the other. This produces a pulse which indicates that a particle has passed through the chamber. Straw tubes are currently being used in several large High Energy Physics (HEP) experiments such as PANDA experiment GSI, ATLAS Transition Radiation Tracker (TRT), etc., as a tracking detector with a low material budget.

4.2 Specifications

4.2.1 The Straw

The structure of a straw tube is shown in Figure 4.1, Straw tube is typically prepared from a kapton film, one side containing a conductive layer of ∼1000-3000 $\mathring{A}$ Al + 4 μm carbon-loaded kapton and the other side containing a thermoplastic polyurethane layer of ∼3 μm. The inner surface of the straw is used as cathode.

The straws are manufactured by the following method. The first step is the preparation of the film, second one is the preparation of the film strips with the width of 8 ± 0.1 mm. Two kapton film tapes (4-8 mm wide) are wound in spiral at a temperature around 200^oC. The thickness of the straw wall is around 60 μm.

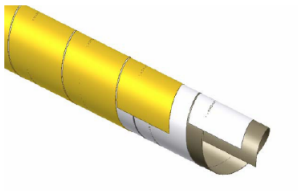

Figure 41: The straw tube [taken from TDR CBM MUCH Report].

4.2.2 Anode wire

The anode used is a gold-plated tungsten (with 2% of rhenium) wire with a 30±0.3 μm diameter (type 861, Luma). The anode wires are centered in the straws by two end plugs and four small plastic spacers. The electrical resistance of this wire is about 60 Ω/m. The wire tension used to set at 70±10 g, close to the elastic limit which is around 1.2 N. The wire should meet following requirements.

- Cross section of the wire should be perfectly circular, variation in diameters in perpendicular directions should not be more than ±2%.
- Wire should be electrically polished to provide a smooth surface free from any defects, a rough surface starts discharge effect soon.
- The base wire surface should also be carefully treated (light electrolytic cleaning) to eliminate all traces of oxides and other possible pollutants just before gold plating.
- The base wire is to be plated with pure gold. No nickel additives to the gold, no Ni-flashing of the wire surface before gold plating are allowed.
- The finished, gold plated wire must have a clean surface which is free of any contaminant, e.g. oil, dirt, dust, fibres, chemical residuals etc. No mechanical treatment of the wire surface is allowed after gold plating [4].

4.2.3 Working principle

When high voltage is applied between the wire and the tube an electric field is generated in the gas filled region. The electric field separates electrons and positive ions produced by an incident charged particle along its trajectory through the gas

volume. The wire is kept at positive voltage and collects the electrons while the ions drift towards the cathode. By choosing thin wires, with a diameter of a few tens of μm, the electric field strength near the wire is made high enough to create an avalanche of electrons. Depending on the high voltage and the gas composition a gain of about $10^4 - 10^5$ can be achieved which is large enough for the observation. The specific energy loss ($\frac{dE}{dx}$) of a charged particle in the straw gas volume can be used to identify the particle species and can be derived from the number of ionization electrons per track length (dx) for the generated straw signal. Main idea of using straw tube in a tracking system is the reduction of material budget [4][8]. Other properties that can be measured by straw tube detector is the drift time of the earliest arriving electrons, one gets the information about the minimum particle track distance from the wire [8].

4.2.4 Gas Mixture

For the good spatial resolution there will be requirement of high anode signals even for the single electron clusters, i.e., requirement of high gain and due to high gain the chamber lifetime decreases. For the optimum gas amplification choice both these factors are kept in mind. It is useful to consider two essentially different situations. The gas mixture is chosen in such a way that even at a low electric field it can effectively quench the electron kinetic energy, preventing them to gain enough energy between collisions. In this case, electrons are in thermal equilibrium with the surrounding medium and the drift velocity is proportional to the electric field. Such gases are usually called "cold" for that given electric field strength. On the contrary, if the electron average kinetic energy differs from the thermal energy, the drift velocity behaviour becomes more complicated. In many gas mixtures the drift velocity becomes saturated and does not depend strongly on the electric field strength. That makes the reconstruction of the track coordinates easier. However, it is difficult to get high spatial resolution in these "hot" gas mixtures, in principle due to the large diffusion. The standard choice of many experiments is to have a "hot" or "warm" gas mixture, that has a weak dependence of the drift velocity on the applied electric field. In this case, the electric field inhomogeneities do not play a significant role, which makes the calibration simpler [8]. An overpressure can be used in these cases to reduce the diffusion. The main requirements, that should be taken into account for the choice of the most suited gas mixture, are:

- good spatial resolution;
- high rate capability;

- radiation hardness;
- radiation length;
- chemical inactivity;
- working voltage;
- working pressure;
- accessibility on the market and price [8].

Keeping all the facts and requirements in mind the study is performed using the Argon and Carbon dioxide gas mixture in the volume ratio of 70:30. In addition this mixture is chosen as Argon is the cheapest noble gas and it also gives escape peak apart from the full energy peak for the 5.9 keV Fe^{55} X-ray energy spectrum for better understanding in terms of the energy.

4.3 Experimental setup

A straw tube prototype obtained from JINR, Dubna, Russia with 6 straws of diameter 6 mm and length 20 cm is used in this study as shown in Figure 4.2. A premixed gas of Argon and CO_2 in 70:30 volume ratio is used in flow mode at a rate of 3 lt/h. The detector is tested using conventional NIM electronics. The positive high

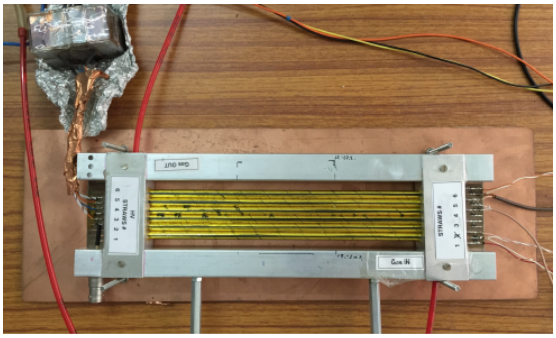

Figure 42: The straw tube prototype.

voltage (HV) is applied to one end of the central wire of the straws using a HV filter box and the signal is collected from the other end through a capacitor using LEMO connector and a charge sensitive preamplifier (VV50) of gain 2m/V/fC and shaping time of 300 ns. Single HV channel is used for each straw tube. A typical Fe^{55} signal

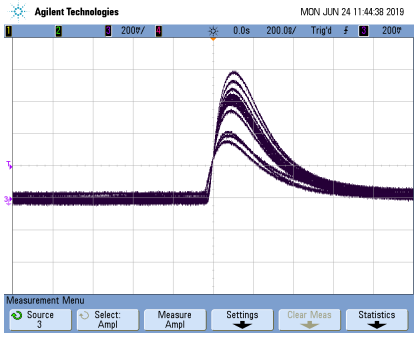

Figure 43: The Fe^{55} signal in the oscilloscope at 1700 V.

in the oscilloscope at 1700 V is shown in Figure 4.3, with settings 200 mV/Div, 200 ns/Div, 50 Ω load. The output signal from the straw after the pre-amplifier is put to a timing SCA (Single Channel Analyzer). The amplifier gain of the SCA is set at 10. The SCA is operated in integral mode and the lower level in the SCA is used as the threshold to the signal. The discriminated TTL signal is fed to a TTL-NIM adapter and the output is counted using a NIM scaler. The count rate (i.e. counts per second) of the detector is then calculated [17]. The block diagram of the electronic setup is given in Figure 4.4.

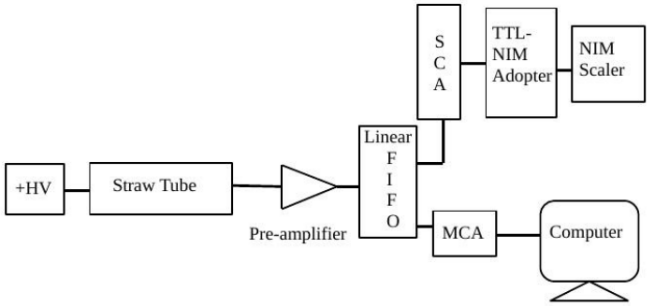

Figure 44: Block diagram of the electronic setup [4].

The study has been performed for two straws out of the six, biasing individually. The source is placed in a perspex source holder. The study is done for different collimator settings of the source holder (different settings corresponds to different rates of radiation).

4.4 Data Analysis and Results

The count rate gain and energy resolution are measured for two straws varying the applied HV using a Fe^{55} X-ray source. First the signal is seen in oscilloscope and a threshold of 200 mV is set after the amplifier to discriminate all the noise.
The collimated source is kept on the straw and for each voltage settings the spectra and count are taken for 1 minute. In case of counts for each voltage settings the background count is also taken for 1 minute removing the source. Typical energy spectra are shown in Figure 4.5, for two different collimator settings and a particular voltages of 1700 V and 1600 V respectively.

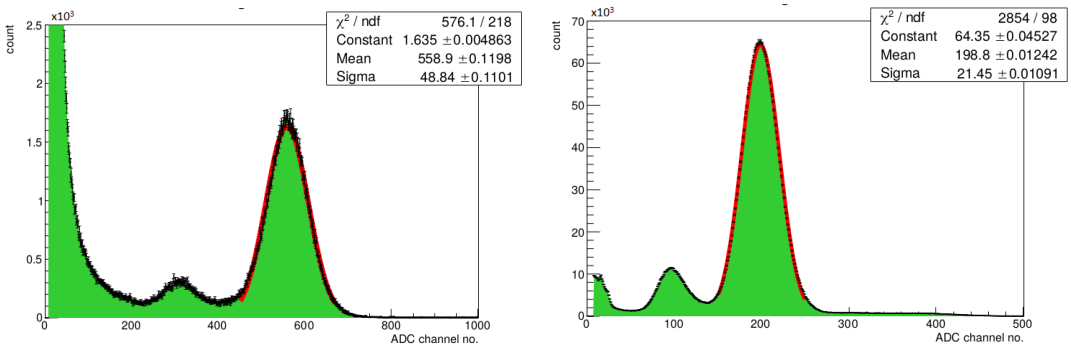

(a) collimator setting 1; Voltage: 1700 V (b) collimator setting 2; Voltage: 1600 V

Figure 45: Typical energy spectrum by a straw tube detecter

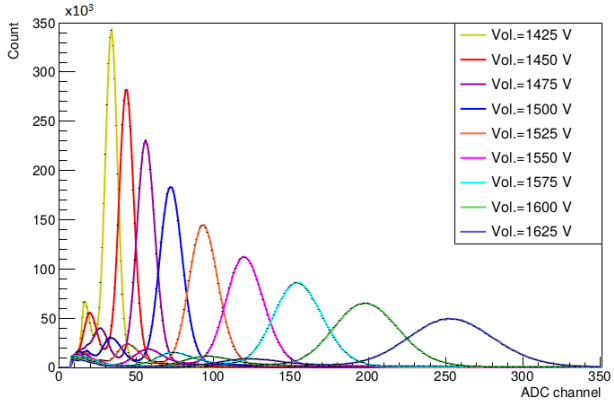

Figure 46: Energy spectra for a straw tube detector varying applied voltage HV.

The 5.9 keV full energy peak, 2.9 keV Argon escape peak and the noise peaks are clearly visible. In the spectra the X-axis are ADC channel number. To convert it to mV ADC is first calibrated with known pulse . Then the conversion factor is found from the pulse height vs ADC channel number calibration curve. For a particular collimator setting these energy spectra with increasing voltage is shown in Figure 4.6, for a particular straw.

All the data are analysed by Root software Package [16]. The variation of the count rate as a function of voltage is shown in Figure 4.7. A plateau in the count rate is observed around 1525 V.

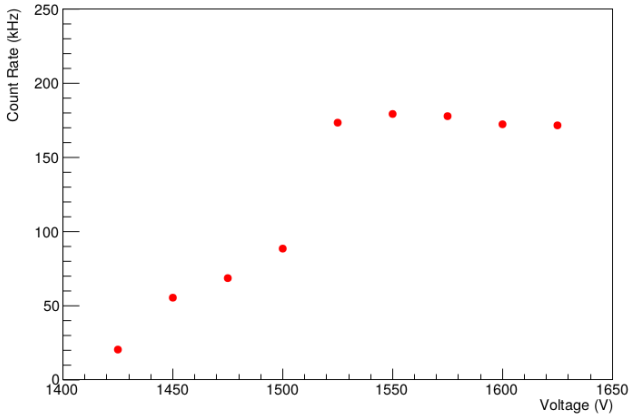

Figure 47: The counting rate as a function of applied HV for Fe^{55} source (Threshold to the SCA : 200 mV).

The gain and energy resolution of the straw tube detector has also been studied. To calculate the gain and energy resolution of the detector the 5.9 keV main peak of the Fe^{55} spectra is fitted with a Gaussian function.
The gain is expressed as:

$$gain = \frac{output\ charge}{input\ charge} = \frac{(pulse\ height/2\ mV)fC}{212 \times eC}$$

Where, pulse height is the mean of the 5.9 keV peak; 2 mV/fC is the preamplifier gain.

The input charge is the primary number of electronic charge produced in the gas detector as a result of total absorption of an X-ray of energy 5.89 keV. For Ar-CO_2 gas in the ratio 70:30 the number of primary electrons produced is 212 approximately.

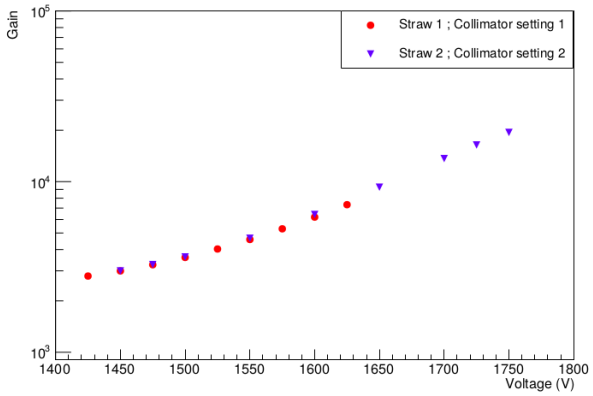

Figure 48: Gain as a function voltage for two straws.

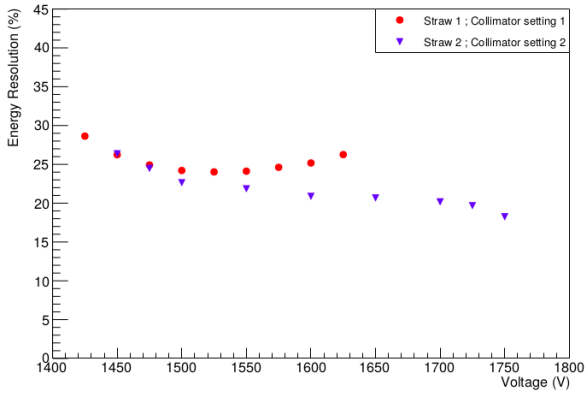

Figure 49: Energy resolution as a function of voltage for two straws.

The input charge is the total charge due to 212 electrons. The energy resolution of the detector is defined as:

$$Energy\ Resolution = \frac{FWHM}{mean} = \frac{2.355 \times sigma}{mean}$$

where, sigma and mean is obtained from the Gaussian fitting of the full energy peak of the spectrum. The gain and energy resolution has been calculated at different bias voltages and for two straws of detector. It is observed that the gain increases exponentially with the voltage and the energy resolution value decreases with voltage as shown in Figure 4.8, 4.9 respectively.

4.5 Summary and outlooks

Basic characteristic studies are performed for straw tube detector with $Ar+CO_2$ gas in 70/30 volume ratio using conventional NIM electronics. In this study count rate, gain, energy resolution are studied. The gain increases exponentially and energy resolution decreases with voltage. Use of the straw tube detector in CBM MUCH is under investigation.

5 Stability Study

5.1 Results of the long term stability study

Long term stability study of the detector prototype has been performed. The variation in the gain of the detector with the temperature and pressure has been studied [4]. The straw has been biased to a high voltage of 1650 V. In this study Ar/CO_2 gas mixture in 70:30 ratio has been used. Using a collimator made of perspex, a circular area on the straw tube detector is exposed with X-ray from a Fe^{55} source which is equivalent to a particle flux of 0.7 MHz/cm^2. The same source has been used to irradiate the detector to obtain the spectrum. The spectra are stored automatically using the ORTEC MCA at an interval of 10 minutes. Since the gain of the gaseous detector depends significantly on the ratio of temperature and pressure (T/p), from the discussion in Section 4.1.

$$G(T/p) = Ae^{(B\frac{T}{p})} \tag{5.1}$$

where the parameters A and B are to be determined from the correlation plot. The temperature (t in ^{o}C) and pressure (p in mbar) are also recorded simultaneously using a data logger. CuteCom software package is used for automatic and continuous monitoring of the temperature and pressure. After setting up all things and applying voltage of 1650 V, the detector is exposed to X-rays from the Fe^{55} source and the energy spectra are recorded. The measurement is continued uninterruptedly for a period of >120 hours.

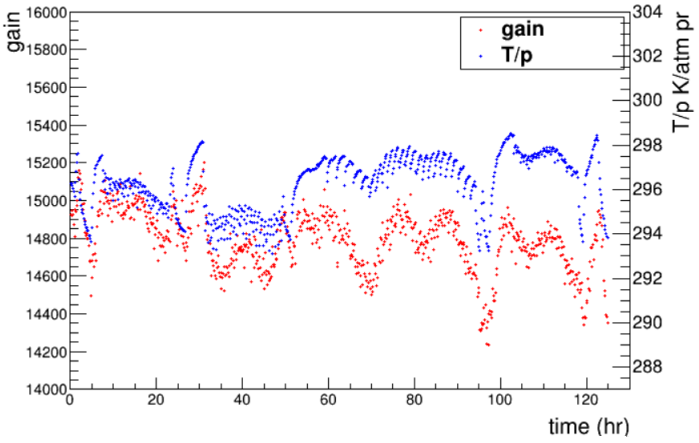

Figure 51: Variation of the measured gain and T/p as a function of the time.

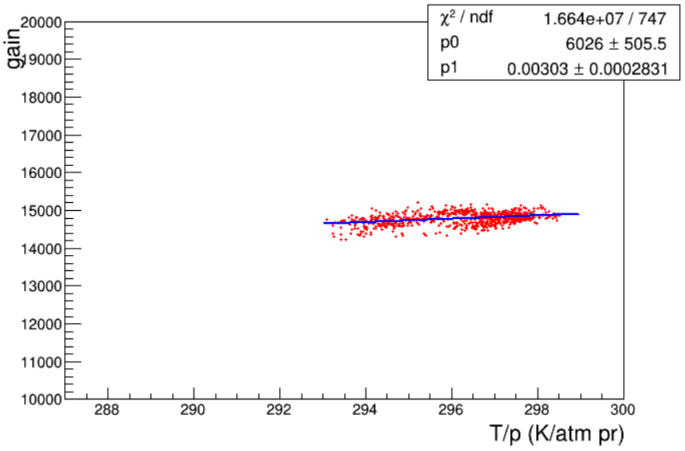

Figure 52: Variation of the gain as a function of T/p (correlation plot).

The variation of the measured gain and T/p are plotted as a function of time in Figure 5.1, where T (= t+273) is the absolute temperature in Kelvin and p (in mbar/1013) is in the unit of atmospheric pressure. The gain vs. T/p correlation plot is drawn and fitted with the function given by equation 5.1 as shown in Figure 5.2 (the parameters A and B are marked as p0 and p1 respectively). After fitting the correlation plot the values of the

the parameters A and B obtained, are 6026±505.5 & 0.0030±0.00028 atm pr/K respectively. Using the fit parameters, the gain is normalised by using the following relation [4]:

$$gain_{normalised} = \frac{gain_{measured}}{Ae^{(B\frac{T}{p})}}$$

To study the stability of the detector, the normalized gain is plotted as a function of the total charge accumulated per unit irradiated area of the straw tube detector. The charge accumulated after radiation exposure in time dt is calculated by

$$\frac{dq}{dL} = \frac{r \times n \times e \times G \times dt}{dL}$$

where, r is the measured rate in Hz incident on a particular length of the detector, dt is the time in seconds, n is the number of primary electrons for a single X-ray photon, e is the electronic charge, G is the gain and dL is the irradiated length.

The normalized gain as a function of the charge accumulated per unit length is shown in Figure 5.3. It can be observed that there is a slight fluctuation in the normalized gain with a mean value ∼1. The distribution of the normalised gain

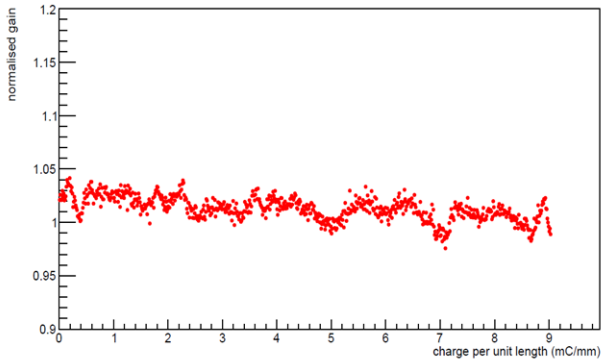

Figure 53: Variation of the normalised gain as a function of the charge per unit length i.e. dQ/dL.

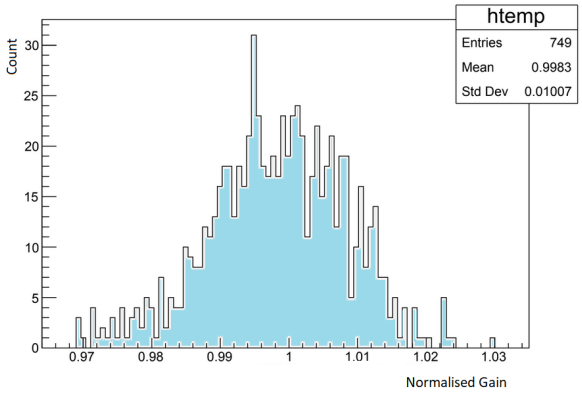

Figure 54: The distribution of the normalised gain.

fitted with a Gaussian function is shown in Figure 5.4. The mean of the Gaussian distribution has been found to be around 0.998 with a sigma of 0.0101 as shown in Figure 5.4.

It can be concluded that the straw tube detector has a stable gain even after a charge accumulation of ∼9 mC/mm.

5.2 Conclusion

A systematic study for the long term stable operation for straw tube detector has been performed using conventional NIM electronics. In this study Ar/CO_2 gas mixture is used in 70/30 volume ratio. Fe^{55} X-ray source of energy 5.9 keV has been used to irradiate the straw tube detector and from the energy spectrum the gain of the detector has been calculated. To check the effect of temperature and pressure on the gain a continuous measurement is performed. Same Fe^{55} X-ray source is used to irradiate the detector and to obtain the spectrum. The measured gain is normalised by T/p corrected gain. The normalised gain is found to be stable with an average value of 0.998 with a sigma of 0.0101 for a duration of $\sim$120 hours, which is equivalent to an accumulation of charge per unit length of 9 mC/mm. Keeping in mind the stability, straw tube is an option to be used in the 3^{rd} and 4^{th} stations of CBM-MUCH. Possibility to use the straw tube detector in CBM MUCH is under investigation.

6 Summary

A detailed study has been performed on the construction, working principle and development of several gaseous detectors. At the Detector Lab of CAPSS, Bose Institute, Research, and Development are being carried out for several detectors such as scintillators, RPC, GEM, and straw tube.

A study of basic characteristics of the straw tube detector in terms of count rate, gain, energy resolution, long-term stability have been performed using Ar+CO_2 gas mixture in the ratio of 70/30. The study have been performed using the 5.9 keV Fe^{55} X-ray source. For any gaseous detector operated in proportional region the gain increases exponentially with voltage and energy resolution decreases with voltage and this feature has been observed for the straw tube detector.

The study of the effect of temperature and pressure and the long term stability test for the straw tube detector has also been performed for a period of more than 120 hours. It has been found that the gain has a strong correlation with the ratio of temperature and pressure. The fit parameters have been calculated using an exponential function. Then the normalized gain has been calculated. The normalized gain as a function of charge accumulated per unit length is a very important figure of merit for the ageing of a gaseous detector. To study the stability of the detector, the normalized gain and its variation with charge accumulation per unit dimension on the detector is usually monitored. It has been observed that for the straw tube detector there is no variation in normalized gain after exposure to radiation for more than 120 hours which is equivalent to a charge per unit length of 9 mC/mm.

References

[1] William R. Leo: Techniques for Nuclear and Particle Physics Experiments, (Second Revised Edition, Springer-Verlag Berlin Heidelberg GmbH)

[2] "Particle Detectors" by William Frass, Lecturer: Dr. Roman Walczak; Michaelmas 2009; Oxford Physics.

[3] "Principles of operation of Multiwire Proportional and Drift Chambers" by F. Sauli, CERN 77-09, 3 May 1997 (Lectures given in the Academic Programme of Cern 1975-1976).

[4] "Studies of the effect of rate on gain for straw tube detector" by S. Roy et al., arXiv:1709.08030

[5] "2-D straw detectors with high rate capability" by N.A. Kuchinskiy et al., arXiv:1502.05363

[6] "The Straw Tube Trackers of the PANDA Experiment" : P. Gianotti et al., arXiv:1307.4537v1

[7] http://www.fair-center.eu/for-users/experiments/cbm.html

[8] PANDA Collaboration, Technical Design Report for the: PANDA Straw Tube Tracker, arXiv:1205.5441

[9] "Radiation detection and measurement" by Glenn F. Knoll; John Wiley & Sons, Inc.

[10] "Particle Detectors", Second Edition, by "Claus Grupen and Boris Shwartz". Cambridge University Press, The Edinburgh Building, Cambridge CB2 8RU, UK.

[11] Technical Design Report for the CBM : Muon Chambers (MuCh), CBM Collaboration (Collaboration author) ; Chattopadhyay, S. (Editor) ; Viyogi, Y. P. (Editor) ; Senger, P. (Editor)* ; Müller, W. F. J. (Editor)* ; Schmidt, C. J. (Editor)* 2015 GSI Darmstadt

[12] "Gaseous Radiation Detectors, Fundamentals and Applications", by Fabio Sauli; Cambridge University Press (2014).

[13] "Experimental Techniques in Nuclear and Particle Physics" by Prof. Stefaan Tavernier, Vrije Universiteit Brussel; Springer.

[14] "Simulation, Design and Construction of a Gas Electron Multiplier for Particle Tracking" by Andrej Sipaj. http://hdl.handle.net/10155/293

[15] Performance Studies of a Micromegas Chamber in the ATLAS Environment - MAMMA Collaboration, JINST 9 (2014) C03016 arXiv:1310.8603

[16] ROOT, A Data Analysis Framework, CERN, website: http://www.root.cern.ch.

[17] "Study of performances of a straw tube detector with high rate" by S. Roy et al, (2018); Nuclear Inst. and Methods in Physics Research, A 936 (2019) 488–490

[18] "Development and characterization of MRPC detectors"; shodhganga.inflibnet.ac.in/bitstream/10603/79589/18/18_chapter%208.pdf